ACS APPLIED MATERIALS & INTERFACES

Research Article

Cite This: ACS Appl. Mater. Interfaces 2019, 11, 18953−18959

www.acsami.org

Iodine-Rich Polymersomes Enable Versatile SPECT/CT Imaging and Potent Radioisotope Therapy for Tumor in Vivo

Jinsong Cao,[†,‡] Yaohua Wei,[†] Yanxiang Zhang,[‡] Guanglin Wang,[*,‡] Xiang Ji,[§] and Zhiyuan Zhong[*,†]

[†]Biomedical Polymers Laboratory, College of Chemistry Chemical Engineering and Materials Science, and State Key Laboratory of Radiation Medicine and Protection and [‡]State Key Laboratory of Radiation Medicine and Protection, School of Radiation Medicine and Protection & School for Radiological and Interdisciplinary Sciences (RAD-X), Collaborative Innovation Center of Radiation Medicine of Jiangsu Higher Education Institutions, Soochow University, Suzhou 215123, P. R. China

[§]Institute of Nuclear Energy Safety Technology, Chinese Academy of Sciences, Hefei 230031, P. R. China

Supporting Information

ABSTRACT: Emerging tumor treatment demands high sensitivity and high-spatial resolution diagnosis in combination with targeted therapy. Here, we report that iodine-rich polymersomes (I-PS) enable versatile single-photon emission computed tomography (SPECT)/computed tomography (CT) dual-modal imaging and potent radioisotope therapy for breast cancer in vivo. Interestingly, I-PS could be easily and stably labeled with radioiodine, ^{125}I and ^{131}I. Dynamic light scattering and transmission electron microscopy showed that ^{125}I-PS had a size of 106 nm and vesicular morphology, similar to those of the parent I-PS. Methyl thiazolyl tetrazolium assays displayed that I-PS and ^{125}I-PS were noncytotoxic, whereas ^{131}I-PS caused significant death of 4T1 cells at 5 mg PS/mL with a radioactivity of 12 μCi. Pharmacokinetic and biodistribution studies showed that ^{125}I-PS has a prolonged circulation and distributes mainly in tumor and the reticuloendothelial system. The intravenous injection of ^{125}I-PS to 4T1 murine breast tumor-bearing mice allowed simultaneous high sensitivity and high-spatial resolution imaging of tumor by SPECT and CT, respectively. The therapeutic studies revealed that ^{131}I-PS could effectively retard the growth of 4T1 breast tumor and significantly prolong mice survival time. The hematoxylin and eosin staining assay proved that ^{131}I-PS induced tumor cell death. I-PS emerges as a robust and versatile platform for dual-modal imaging and targeted radioisotope therapy.

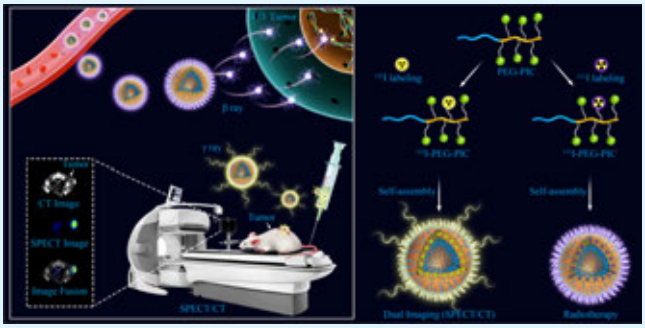

KEYWORDS: *polymersomes, contrast agents, SPECT/CT, theranostics, radioisotope*

INTRODUCTION

Relying on the high sensitivity and high-spatial resolution diagnosis, combined therapy has attracted great attention in recent years.[1,2] Single-photon emission computed tomography (SPECT) with a high sensitivity and functional imaging is widely used for cancer theranostics.[3] Owing to the limitation of the anatomical information of SPECT imaging, X-ray computed tomography (CT) has been widely conducted for patient imaging due to its high spatial and density resolution and its ability to provide the information on anatomic structure.[4,5] However, compared to SPECT imaging, CT imaging lacks sufficient sensitivity and molecular information. To overcome the limitations of single-modal imaging, dual- and multimodal imaging has attracted great attention.[6−10] For instance, ^{99m}Tc-labeled dendrimer-entrapped gold nanoparticles,[11−14] ^{99m}Tc-labeled dendrimer with iodine,[15] and ^{153}Sm-labeled lanthanide-based nanoparticles[16,17] have recently been designed and investigated for in vivo SPECT/CT imaging. These reported nanocontrast agents exhibited significant improvements of both SPECT and CT signals in tumor, sentinel lymph node, and atherosclerosis plaques. However, a huge dose of CT contrast agents is needed for improving the imaging sensitivity. On the other hand, given the potential toxicity, it is very difficult to translate inorganic CT contrast agents to clinical applications. It is impendent to develop multifunctional contrast agents for multimodal imaging.

Theranostics that combines diagnostics and therapy has received widespread interests as future personalized medicine.[18−24] Polymersomes with a vesicular structure as for liposomes are able to deliver hydrophilic and hydrophobic imaging agents and drugs, offering a versatile platform for theranostics. Compared to liposomes, polymersomes are more stable and easier to fabricate with tunable properties.[25−29] Notably, nanosized polymersomes can target tumor through the enhanced permeation retention (EPR) effect ("passive targeting").[30,31] Various imaging agents such as fluorescent

Received: March 10, 2019
Accepted: May 7, 2019
Published: May 7, 2019

DOI: 10.1021/acsami.9b04294
ACS Appl. Mater. Interfaces 2019, 11, 18953−18959

Scheme 1. Schematic Illustration Showing the Preparation of Radiolabeled Iodine-Rich Polymersomes, ^{125}I-PS and ^{131}I-PS[a]

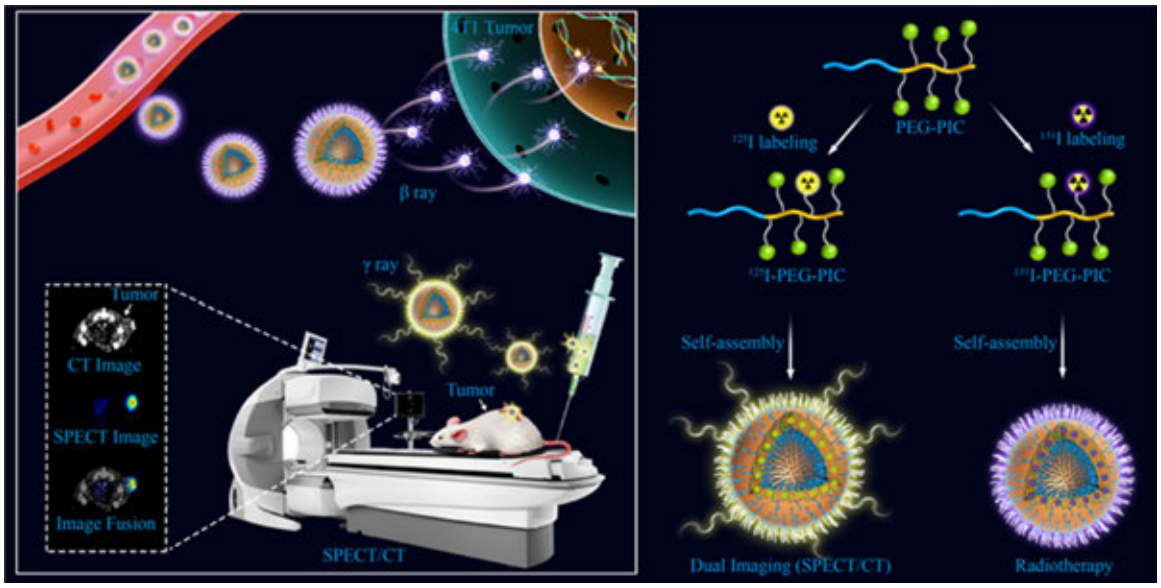

[a]^{125}I-PS for SPECT/CT dual-mode imaging and ^{131}I-PS for radioisotope therapy of cancer. PEG-PIC is an abbreviation of poly(ethylene glycol)-*b*-poly(iodinated carbonate) copolymer.

dyes, magnetic particles, quantum dots, and radionuclides have been integrated with polymersomes.[32−38] Polymersomes have also been employed for loading different drugs, including chemotherapeutics, proteins, and siRNA, for cancer treatment.[39−42] Drugs loaded in polymersomes exhibited enhanced tumor accumulation and significantly improved anticancer efficacy. Notably, the integration of polymersomes with radionuclides labeling for radioisotope therapy has not yet been reported as per our knowledge.

Over the past years, different iodine-rich polymers and nanoparticles have been developed for CT imaging in that they provide several advantages over small molecule contrast agents like preventing fast renal excretion, reducing iodine hypersensitivity, prolonging circulation time, and achieving targeted imaging.[43−47] In our recent work, we have reported that iodine-rich nanopolymersomes (I-PS) have shown great X-ray attenuation ability.[48] Compared with Iohexol, a commercial X-ray contrast agent, I-PS possesses strong CT signals in the blood pool, reticuloendothelial system, and several malignant tumors of mice after intravenous injection. In this work, we further develop I-PS as a multimodal contrast agent for versatile SPECT/CT imaging and potent radioisotope therapy for tumor in vivo (Scheme 1). ^{131}I has been used for radioisotope therapy as it emits high-energy β particles that can cause cell DNA strand breaks and induce cell death, whereas ^{125}I is mostly used for imaging as it emits Auger electron that can cause DNA strand breaks only when it is close to the cell nucleus.[49−51] With radiolabeling, ^{125}I- and ^{131}I-labeled I-PS were able to achieve high-efficiency CT imaging and SPECT imaging, as well as radioisotope therapy for tumors. This represents a first report on radiolabeled polymersomes for dual-modal imaging-guided radioisotope therapy.

MATERIALS AND METHODS

Chemicals. Radioiodine (Na^{125}I and Na ^{131}I) was supplied by Shanghai GMS Pharmaceutical Co., Ltd. Acetic acid, dimethyl formamide, and ethanol were bought from Sinopharm Chemical Reagent Co., Ltd. All chemicals and reagents were used as received.

Synthesis of PEG-PIC (^{125}I) and PEG-PIC (^{131}I). Poly(ethylene glycol)-*b*-poly(iodinated carbonate) (PEG-PIC) with an M_n of 5.0−50.0 kg/mol was synthesized as previously reported.[48] For the synthesis of PEG-PIC (^{125}I), Na^{125}I (500 μCi, 370 mCi/mL) was mixed with ethanol (270 μL) and evaporated at 85 °C by a thermo shaker. PEG-PIC (1 mg) and acetic acid (2 μL) in dimethyl formamide (DMF) (200 μL) were added to the dry Na^{125}I (iodine in PEG-PIC/Na^{125}I molar ratio = 2.08 × 10^3) and heated to 70 °C with varied time from 1 to 10 h under shaking. The radiochemical yield was measured by a thin-layer chromatography assay using saline as a mobile phase. The R_f of ^{125}I-PS was ∼0.1, and the R_f of free ^{125}I was ∼0.9. PEG-PIC (^{131}I) was obtained by the same method.

Preparation of ^{125}I-PS and ^{131}I-PS. ^{125}I-PS and ^{131}I-PS were prepared by a solvent exchange method. In a typical example, 200 μL of PEG-PIC (^{125}I) solution in DMF (5 mg/mL) was added dropwise to 800 μL of deionized water. To remove free Na^{125}I and DMF, the resulting ^{125}I-PS dispersion was dialyzed against 200 mL of deionized water for 8 h with three times change of deionized water (MWCO = 8000 Da) and concentrated by ultrafiltration (Millipore, MWCO =10 kDa) at the speed of 4500 rpm for 10 min. ^{131}I-PS and I-PS were obtained using the same method.

The hydrodynamic radii of I-PS and ^{125}I-PS were measured by dynamic light scattering (DLS). All experiments were performed on a Malvern Zetasizer Nano ZS90 equipped with a solid-state He−Ne laser (λ = 633 nm) in triplicate at 25 °C. A transmission electron microscope (TEM) (FEI Tecnai F20) was used to measure the size and morphology of ^{125}I-PS, manipulating at 120 kV. ^{125}I-PS (10 μL, 1 mg/mL) was dropped onto a carbon-coated copper grid of 200 mesh, and the redundant liquid was removed using a filter paper after 5 min. Aqueous solution of phosphotungstic acid (10 mg/mL, 10 μL) was dropped onto the copper grid to dye the ^{125}I-PS.

Cytotoxicity Assay of ^{125}I-PS and ^{131}I-PS. Methyl thiazolyl tetrazolium (MTT) assays were used to evaluate the cytotoxicities of ^{125}I-PS and ^{131}I-PS. 4T1 cells were seeded and cultured in a 96-well plate (1 × 10^4 cells/well) in DMEM with 10% fetal bovine serum at 37 °C for 24 h in a 5% CO_2 atmosphere. The medium was aspirated and replaced by I-PS, ^{125}I-PS, and ^{131}I-PS with different concentrations (0.31, 0.63, 1.25, 2.5, and 5 mg/mL corresponding to radioactivities of 0.75, 1.5, 3, 6, and 12 μCi/mL) at 37 °C for 24 h. The cells were cultured with 3-(4,5-dimethylthiazol-2-yl)-2,5-diphenyltetrazolium bromide solution (100 μL, 0.5 mg/mL) for 4 h before the addition of dimethyl sulfoxide (100 μL). A microplate

DOI: 10.1021/acsami.9b04294
ACS Appl. Mater. Interfaces 2019, 11, 18953−18959

reader (Thermo, Varioskan Flash) was used to measure the absorption of each solution.

In Vitro and in Vivo Dual-Modal Imaging. In vitro and in vivo dual-modal imaging was performed on a microSPECT/CT scanner (Milabs, Utrecht, the Netherlands) with a multipinhole focused collimator. The SPECT was performed for 15 min per scan with an energy window from 20 to 40 keV. The parameter of the CT scan was set as an accurate mode using three frames averaging, full angle, with 55 kV tube voltage and 615 mA tube current. To evaluate the in vitro performance of dual-modal imaging, concentrations of ^{125}I-PS varied from 0 to 6.25, 12.5, 18.75, and 25 mg/mL, which corresponded to radioactivities of 0, 6.25, 12.5, 18.75, and 25 μCi in tube phantom.

All animal experiments were operated following a protocol approved by the Animal Care and Use Committee of Soochow University. Female BALB/c mice (6 weeks of age, 20−23 g per animal) of specific pathogen-free grade were received from Shanghai SLAC Laboratory Animal Co., Ltd. The breast tumor model was established by subcutaneous injection of 4T1 cell suspension (~5 × 10^6 cells) into the flank region of the right back of mice, and the consequent tumor was allowed to grow for 10 days. 4T1 tumor-bearing mice were injected with ^{125}I-PS (1000 mg/kg, 200 μCi) by intravenous injection though the tail vein without thyroid preblocking. The 1.5% isoflurane/oxygen gas mixture (flow rate: 0.6 L/min) was used to anesthetize the mice by inhalation on a temperature-controlled animal bed of the microSPECT/CT, scanned with varied times (0, 4, 6, 8, 12, 24, and 48 h). To study the retention of ^{125}I-PS in tumor, the acquisition times of 4T1 tumor-bearing mice were scanned at 2, 6, 10, 14, 24, 48, 72, 96, 144, and 192 h postinjection. All microSPECT/CT data were handled with POMD (version 3.602) software.

Blood Circulation and Biodistribution. For in vivo pharmacokinetic studies, blood samples were collected from the retinal veins of healthy BALB/c mice (n = 3) after postinjection of ^{125}I-PS at 0, 1, 2, 4, 6, 8, 24, and 48 h, respectively. The blood samples were weighed, and the radioactivity was measured by a γ counter (Multi Crystal LB 2111 γ counter). To study the biodistribution of ^{125}I-PS, major organs (heart, kidneys, liver, lungs, and spleen) were weighed and the radioactivity was measured.

In Vivo Therapy. 4T1 tumor-bearing BALB/c mice (30−50 mm^3) were randomly divided into two groups: I-PS and ^{131}I-PS (200 μCi, 50 mg/kg). The above agents were intravenously injected every 4 days at days 0, 4, 8, and 12 without thyroid preblocking. The tumor volume was monitored by a caliper every 2 days and calculated according to the following equation: $V = LW^2/2$, where L and W are the length and width of the tumor, respectively. Data on body weight and death rate were recorded to evaluate the treatment performance. The relative tumor volume was calculated by V/V_0, where V_0 means the tumor volume on day 0. For histological analysis staining, tumor and major organs were harvested, fixed in 10% neutral buffered formalin, and embedded in paraffin. The tumor then was sectioned into thin slices and stained with hematoxylin and eosin (H&E).

Statistical Analysis. All data were presented as mean ± standard deviation. One-way analysis of variance (ANOVA) was used to assess the significance between groups, after which posthoc tests with the Bonferroni correction were used for comparison among individual groups. *p < 0.05 was considered significant, and **p < 0.01 and ***p < 0.001 were considered highly significant.

RESULTS AND DISCUSSION

Preparation and Cytotoxicity of Radioactive Iodine-Rich Polymersomes. An iodine-rich polymer, PEG-PIC, was synthesized with an M_n of 5.0−50.0 kg/mol, which corresponded to an iodine content of 60.4 wt %, according to our previous protocols.[48] PEG-PIC was radiolabeled with, radioisotopes, ^{125}I and ^{131}I, via isotopic exchange in dimethyl formamide (DMF) solution at 80 °C using acetate acid as a catalyst (Figure 1A). As shown in Figure 1B, the ^{125}I radiolabeling efficiency increased with the increasing time.

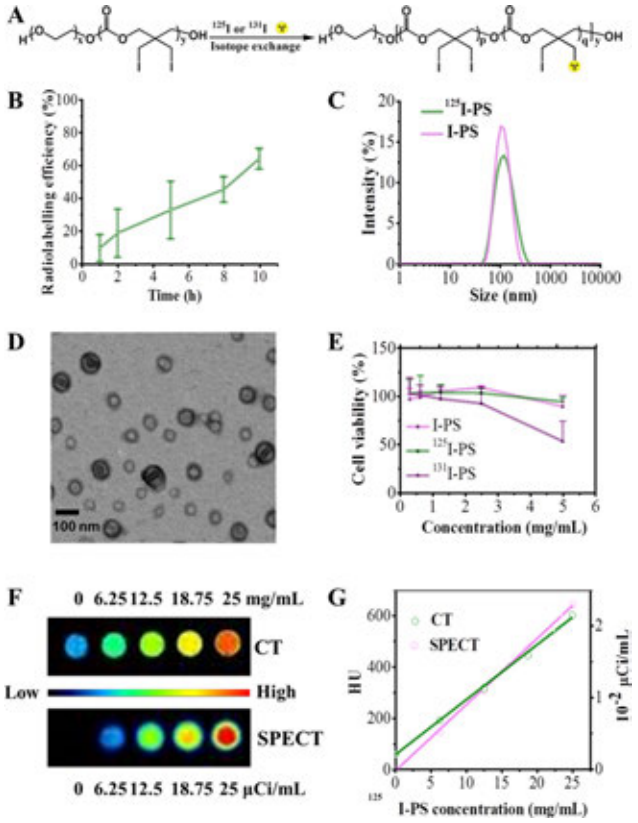

Figure 1. Synthesis and characterization of radiolabeled polymersomes. (A) Synthesis of PEG-PIC (^{125}I) and PEG-PIC (^{131}I) by isotopic exchange. (B) Radiolabeling efficiency as a function of time. The iodine exchange reaction was carried out with 200 μCi Na^{125}I in DMSO at 80 °C. (C) Size distribution profiles of I-PS and ^{125}I-PS measured by DLS. (D) TEM image of ^{125}I-PS. (E) MTT assays of I-PS, ^{125}I-PS, and ^{131}I-PS at polymer concentrations varying from 0.31 to 5 mg/mL in 4T1 cells following 48 h incubation (n = 6) (corresponding ^{125}I-PS and ^{131}I-PS radioactivities varying from 0.75 to 12 μCi). (F) Phantoms reconstructions of ^{125}I-PS measured at polymer concentrations varying from 1 to 25 mg/mL (the corresponding radioactivity varying from 0 to 25 μCi). (G) Quantification of CT and SPECT from phantoms reconstructions.

The maximum radiolabeling yield was measured to be 63.9 ± 6.3% through the thin-layer chromatography assay. The radiolabeling efficiency of ^{131}I-PS was similar to that of ^{125}I-PS (Figure S1). ^{125}I-labeled PEG-PIC readily formed polymersomes in water. Similar to nonradioactive I-PS, the dynamic size of ^{125}I-PS was 106 nm, as determined by the dynamic light scattering (DLS) assay (Figure 1C). Transmission electron microscopy (TEM) imaging showed that ^{125}I-PS had a spherical vesicular structure with an average size of 80 nm, which was close to the DLS data (Figure 1D). Hence, the isotopic exchange, with radioisotopes such as ^{125}I and ^{131}I, has not changed the intrinsic properties of iodine-rich polymersomes. We further tested the radiostabilities of ^{125}I-PS and ^{131}I-PS in PBS and 10% serum. The results showed a little loss of ^{125}I and ^{131}I in 48 h (Figures S2 and S3), confirming a high radiostability. This radiolabeling strategy is easy, fast, and stable.

Prior to the in vivo evaluation, we first investigated the potential cytotoxicities of I-PS, ^{125}I-PS, and ^{131}I-PS in murine 4T1 breast cancer cells by the methyl thiazolyl tetrazolium (MTT) assay. No obvious toxicity to the 4T1 cells was

DOI: 10.1021/acsami.9b04294
ACS Appl. Mater. Interfaces 2019, 11, 18953−18959

observed even at a concentration of 5 mg/mL for I-PS. Notably, similar to nonradioactive I-PS, ^{125}I-PS was practically nontoxic to 4T1 cells even at a high concentration of 5 mg/mL, which corresponded to a radioactivity of 12 μCi (Figure 1E), suggesting that ^{125}I-PS has good safety. The lack of cytotoxicity of ^{125}I-PS is likely due to its low dose, as ^{125}I causes DNA strand break via the Auger electron that works only when it is close to the cell nucleus. With ^{125}I, both high dose and nuclear entry are required for effective radiotherapy. However, ^{131}I-PS caused obvious toxicity to 4T1 cells due to the released β rays from ^{131}I. The immunofluorescence cell experiments further confirmed that ^{131}I-PS caused the DNA double strand breaks, while I-PS and ^{125}I-PS did not (Figure S4). Therefore, ^{125}I-labeled I-PS might be used for SPECT/CT imaging of mice bearing 4T1 tumors, whereas ^{131}I-labeled I-PS might act as a therapeutic agent for radioisotope therapy of tumor.

In Vitro and in Vivo SPECT/CT Dual-Modal Imaging. In our previous work, I-PS with a remarkably high iodine content of 60.4 wt % was demonstrated to be an excellent CT contrast agent compared with the commercial contrast agent Iohexol.[48] To explore the potential of ^{125}I-PS for dual-modal imaging, we performed in vitro SPECT/CT scan by tube phantoms. It was found that the intensity of reconstructed images of both CT and SPECT increased by increasing the concentration of I-PS and ^{125}I radioactivity, respectively. The CT and SPECT images matched well with each other (Figure 1F). The quantitative analysis showed that the X-ray attenuation value increased from 192.4 HU to 602 HU with increasing the concentration of ^{125}I from 6.25 to 25 mg/mL, owing to the large attenuation of X-rays by the iodine atom.[43−46] The radioactivity intensity of ^{125}I-PS increased linearly from 0.52 × 10^{-2} to 2.3 × 10^{-2} μCi/mL from the SPECT imaging assay (Figure 1G). The phantom studies suggested that the developed ^{125}I-PS could be used for SPECT and CT dual-modal imaging.

To study the in vivo performance of ^{125}I-PS, SPECT and CT dual-modal imaging of ^{125}I-PS in mice bearing 4T1 tumor were conducted. The three-dimensional (3D) images of SPECT showed that ^{125}I-PS exhibited whole body distribution after injection. After 48 h of injection, ^{125}I-PS showed high tumor accumulation (Figure 2A). Notably, ^{125}I-PS also showed a high accumulation in the liver and spleen. By installing a tumor-targeting ligand such as an antibody and a peptide on ^{125}I-PS, we might reduce its accumulation in the liver and spleen and further increase its tumor accumulation. On the other hand, not any radioactivity signal in thyroid of mice with ^{125}I-PS treatment was detected, further demonstrating the excellent stability of our ^{125}I-PS in vivo. Notably, SPECT imaging only detects the radioisotope. We performed the CT imaging to locate the nanoparticles. As expected, CT imaging of mice also showed a high tumor accumulation after 48 h of injection. The CT imaging was in good accordance with the SPECT imaging (Figure 2B). The X-ray attenuation value of the tumor increased from 66 ± 3 HU at 0 h to 256 ± 3 HU at 48 h postinjection (Figure 2C). Compared to currently used small molecular contrast agents, ^{125}I-PS provides a significantly longer detection window. Interestingly, quantitative SPECT measurements showed that the radioactivity intensity of tumor tissue increased from 2 ± 0.45% ID/g (percentage of injected dose per gram of tissue) at 0.5 h postinjection up to 17.45 ± 0.08% ID/g at 48 h postinjection (Figure 2D), confirming that I-PS can target 4T1. The high tumor accumulation of ^{125}I-PS is

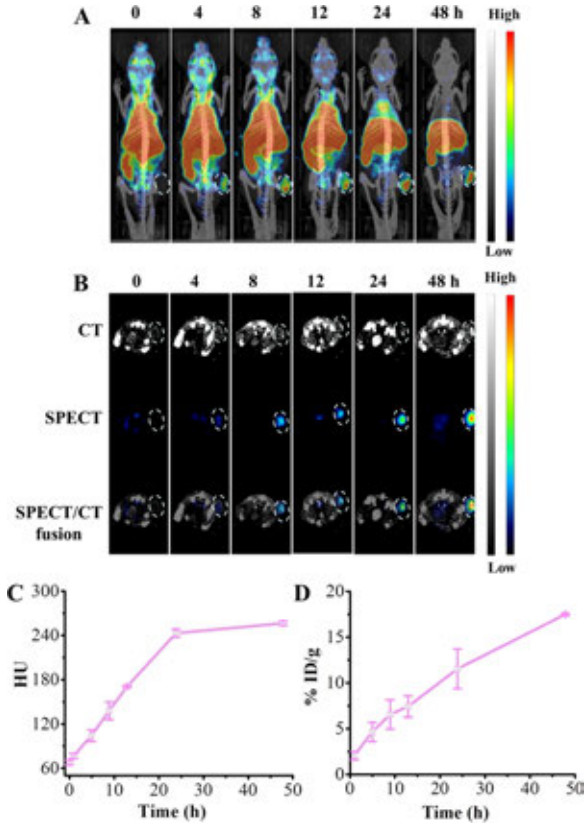

Figure 2. In vivo microSPECT/CT dual-modal imaging of 4T1 tumor-bearing BALB/c mice at 0, 4, 8, 12, 24, and 48 h postinjection of ^{125}I-PS. (A) 3D images of mice (4T1 tumor xenograft at right backleg). (B) Coronal section of CT, SPECT, and fusion images of mice (tumors marked with dashed circles). Tumor uptake quantified by CT (C) and SPECT (D).

likely due to a high vascularization of 4T1 tumor, as well as good stability and long circulation time of ^{125}I-PS, both critical to the observed EPR effect.[52−54] The above results demonstrate that ^{125}I-PS can be used as a contrast agent for dual-modal imaging. Of note, it is a practical challenge to balance the dose for dual-modal imaging due to difference in sensitivity. Here, I-PS can uniquely meet the dose requirements for SPECT and CT dual-modal imaging in that we can tailor ^{125}I-PS radioactivity to make it suitable for both SPECT and CT imaging.

Pharmacokinetics and Biodistribution. To study the in vivo behaviors of nanoparticles, healthy mice were intravenously injected with ^{125}I-PS without thyroid preblocking. After different time points, the blood sample was collected from the retinal vein for the radioactivity assay by the γ counter. The results showed that ^{125}I-PS exhibited long blood circulation time with pharmacokinetics followed a two-compartment model with the first- and second-phase blood circulation half-lives calculated to be 0.88 h ($t_{1/2\alpha}$) and 10.5 h ($t_{1/2\beta}$), respectively (Figure 3A). In contrast, free Na^{125}I showed significant accumulation in the thyroid and was rapidly cleared from the systemic circulation through kidneys after intravenous injection (Figure S5).

We further studied the biodistribution of ^{125}I-PS in 4T1 tumor-bearing mice. The tumor and major organs were excised at 48 h post intravenous injection of ^{125}I-PS (1000 mg/kg, 200 μCi) via the tail vein. The radioactivity assays confirmed a high tumor accumulation of ^{125}I-PS (17.4 ± 0.1% ID/g), which was

DOI: 10.1021/acsami.9b04294
ACS Appl. Mater. Interfaces 2019, 11, 18953−18959

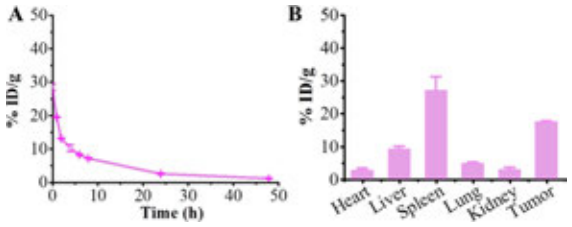

Figure 3. (A) Pharmacokinetics of ^{125}I-PS in mice following iv injection (n = 3). (B) Biodistribution of ^{125}I-PS in 4T1 tumor-bearing BALB/c mice at 48 h postinjection (n = 3).

significantly higher than that in the healthy organs such as the heart, liver, lung, and kidneys, except for the spleen (Figure 3B). Figure S6 shows that ^{125}I-PS could be slowly excreted from the body with time. ^{125}I-PS is most likely degraded by enzymatic pathway in vivo, as reported for poly(trimethylene carbonate) and copolymers.[55,56] The long circulation and favorable biodistribution make I-PS an interesting nanosystem for radioisotope therapy.

In Vivo Therapy. To assess the frequency of administration, we first monitored ^{125}I-PS in vivo for several days. As shown in Figure 4, tumor uptake of ^{125}I-PS reached a plateau

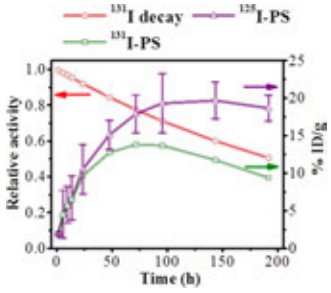

Figure 4. Tumor uptake of ^{131}I-PS predicted by ^{125}I-PS.

on day 4 after injection. Combined with the half-life of ^{131}I, tumor uptake of ^{131}I-PS would reach the maximum on day 4 and then decrease. Under the guidance of SPECT/CT dual-modal imaging, in vivo radioisotope therapy was conducted. Mice bearing 4T1 tumors were randomly divided into two group (n = 5): I-PS and ^{131}I-PS. ^{131}I-PS was intravenously injected into mice every 4 days with a radioactivity of 200 μCi and total four injections were given at days 0, 4, 8 and 12. Notably, ^{131}I-PS significantly inhibited tumor growth compared to that of the radioinactive I-PS control (Figure 5A). Moreover, Kaplan−Meier survival curves showed that the mice treated with ^{131}I-PS had a significantly longer median survival time than that of the control group (32 versus 14 days) (Figure 5B). Meanwhile, ^{131}I-PS did not induce much loss of body weight compared to that for I-PS, demonstrating that ^{131}I-PS does not cause significant side effects (Figure 5C). Histological assays further revealed that the tumor tissues from ^{131}I-PS treated mice exhibited remarkable cell necrosis, whereas I-PS induced no obvious toxicity to cancer cells (Figure 5D). It should be further noted that little damage was observed in the normal tissues of ^{131}I-PS-treated mice, further suggesting that ^{131}I-PS possesses good safety (Figure S7). Therefore, iodine-rich polymersomes enable not only SPECT/CT dual-modal imaging but also potent radioisotope therapy of breast cancer in vivo.

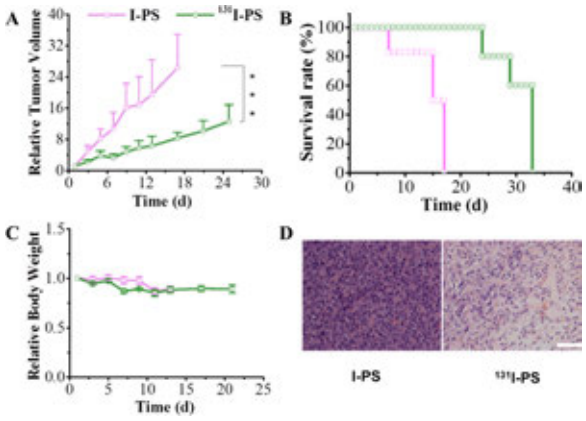

Figure 5. In vivo antitumor performance of ^{131}I-PS in 4T1 tumor-bearing mice. ^{131}I-PS was given on days 0, 4, 8, and 12 at a radioactivity of 200 μCi (n = 5). (A) 4T1 tumor growth rate. Statistical analysis: one-way ANOVA with Tukey's multiple comparison tests, ***p < 0.001. (B) Survival curves of mice within 32 days. (C) Body weight changes of mice. (D) Macroscopic images of H&E-stained sections of tumors excised on day 2. The scale bar corresponds to 100 μm.

CONCLUSIONS

We have demonstrated that iodine-rich-polymersomes (I-PS) can be used for SPECT/CT dual-modal imaging as well as radioisotope therapy for 4T1 murine breast cancer in BALB/c mice. Interestingly, I-PS with high-efficiency and stable radiolabeling with ^{125}I or ^{131}I shows similar biophysical properties to those of the parent I-PS. As for I-PS, ^{125}I-PS is nontoxic, whereas ^{131}I-PS shows pronounced toxicity to 4T1 breast cancer cells. ^{125}I-PS provides effective and simultaneous contrast enhancement in tumor in vivo in both SPECT and CT imaging with a remarkable tumor accumulation of 17.45 ± 0.08% ID/g observed at 48 h postinjection. The therapeutic studies clearly show that ^{131}I-PS effectively inhibits tumor growth without inducing obvious side effect. These iodine-rich polymersomes enabling SPECT/CT dual-modal imaging and radioisotope therapy provide a novel and unique platform for cancer theranostics.

ASSOCIATED CONTENT

Supporting Information

The Supporting Information is available free of charge on the ACS Publications website at DOI: 10.1021/acsami.9b04294.

Immunofluorescence cell experiment; radiolabeling efficiency as a function of time; radiostabilities of ^{125}I-PS and ^{131}I-PS; DNA damage analysis of 4T1 cells following treatment with I-PS, ^{125}I-PS, or ^{131}I-PS; 3D images of 4T1 tumor-bearing mice of Na(^{125}I) and ^{125}I-PS; and H&E stain sections of major organs (PDF)

AUTHOR INFORMATION

Corresponding Authors

*E-mail: glwang@suda.edu.cn. Tel: +86-512-65880054 (G.W.).

*E-mail: zyzhong@suda.edu.cn. Tel: +86-512-65880098 (Z.Z.).

ORCID

Zhiyuan Zhong: 0000-0003-4175-4741

DOI: 10.1021/acsami.9b04294
ACS Appl. Mater. Interfaces 2019, 11, 18953−18959

Notes

The authors declare no competing financial interest.

■ ACKNOWLEDGMENTS

This work was supported by the National Key Research Program of China (2016YFC0101200), the National Natural Science Foundation of China (51603139, 81720108024), the Natural Science Foundation of Jiangsu Province (BK20160307), the Natural Science Foundation of Anhui Province (1508085SME220), the China Postdoctoral Science Foundation (2016M591915, 2018T110547), and Suzhou Administration of Science & Technology (SYS201701).

■ REFERENCES

(1) Weissleder, R. Molecular Imaging in Cancer. *Science* **2006**, *312*, 1168−1171.
(2) Weissleder, R.; Pittet, M. Imaging in the Era of Molecular Oncology. *Nature* **2008**, *452*, 580−589.
(3) Singh, R.; Patel, K.; Leong, K.; Kim, H. Progress in Nanotheranostics Based on Mesoporous Silica Nanomaterial Platform. *ACS Appl. Mater. Interfaces* **2017**, *9*, 10309−10337.
(4) Lusic, H.; Grinstaff, M. X-ray-computed Tomography Contrast Agents. *Chem. Rev.* **2013**, *113*, 1641−1666.
(5) Li, X.; Anton, N.; Zuber, G.; Vandamme, T. Contrast Agents for Preclinical Targeted X-ray Imaging. *Adv. Drug Delivery Rev.* **2014**, *76*, 116−133.
(6) Lee, S.; Jeon, S.; Jung, S.; Chun, I.; Ahn, C. Targeted Multimodal Imaging Modalities. *Adv. Drug Delivery Rev.* **2014**, *76*, 60−78.
(7) Wang, S.; Lin, J.; Wang, Z.; Zhou, Z.; Bai, R.; Lu, N.; Liu, Y.; Fu, X.; Jacobson, O.; Fan, W.; Qu, J.; Chen, S.; Wang, T.; Huang, P.; Chen, X.; et al. Core-satellite Polydopamine Gadolinium Metallofullenren Nanotheranostics for Multimodal Imaging Guided Combination Cancer Therapy. *Adv. Mater.* **2017**, *29*, No. 1701013.
(8) Cheng, K.; Chen, H.; Jenkins, C.; Zhang, G.; Zhao, W.; Zhang, Z.; Han, F.; Fung, J.; Yang, M.; Jiang, Y.; Xing, L.; Cheng, Z. Synthesis, Characterization, and Biomedical Applications of a Targeted Dual-modal Near-infrared-II Fluorescence and Photoacoustic Imaging Nanoprobe. *ACS Nano* **2017**, *11*, 12276−12291.
(9) Yu, B.; Wei, H.; He, Q.; Ferreira, C.; Kutyreff, C.; Ni, D.; Rosenkrans, Z.; Cheng, L.; Yu, F.; Egnle, J.; Lan, X.; Cai, W. Efficient Uptake of ^{177}Lu-phorphyrin-PEG Nanocomplexes by Tumor Mitochondria for Multimodal-imaging Guided Combination Therapy. *Angew. Chem., Int. Ed.* **2018**, *57*, 218−222.
(10) Tang, J.; Zhou, H.; Liu, J.; Liu, J.; Li, W.; Wang, Y.; Hu, F.; Huo, Q.; Li, J.; Liu, Y.; Chen, C. Dual-mode Imaging-guided Synergistic Chemo- and Magnetohyperthermia Therapy in a Versatile Nanoplatform to Eliminate Cancer Stem Cells. *ACS Appl. Mater. Interfaces* **2017**, *9*, 23497−23507.
(11) Zhou, B.; Wang, R.; Chen, F.; Zhao, L.; Wang, P.; Li, X.; Banyai, I.; Ouyang, Q.; Shi, X.; Shen, M. ^{99m}Tc-labeled RGD-polyethylenimine Conjugates with Entrapped Gold Nanoparticles in the Cavities for Dual-mode SPECT/CT Imaging of Hepatic Carcinoma. *ACS Appl. Mater. Interfaces* **2018**, *10*, 6146−6154.
(12) Xu, X.; Zhao, L.; Li, X.; Wang, P.; Zhao, J.; Shi, X.; Shen, M. Targeted Tumor SPECT/CT Dual Mode Imaging Using Multifunctional RGD-modified Low Generation Dendrimer-entrapped Gold Nanoparticles. *Biomater. Sci.* **2017**, *5*, 2393−2397.
(13) Wen, S.; Zhao, L.; Zhao, Q.; Li, D.; Liu, C.; Yu, Z.; Shen, M.; Majoral, J.; Mignani, S.; Zhao, J.; Shi, X. A Promising Dual Mode SPECT/CT Imaging Platform Based on ^{99m}Tc-labeled Multifunctional Dendrimer Entrapped Gold Nanoparticles. *J. Mater. Chem. B* **2017**, *5*, 3810−3815.
(14) Li, X.; Xiong, Z.; Xu, X.; Luo, Y.; Peng, C.; Shen, M.; Shi, X. ^{99m}Tc-labeled Multifunctional Low-generation Dendrimer-entrapped Glod Nanoparticles for Targeted SPECT/CT Dual-mode Imaging of Tumors. *ACS Appl. Mater. Interfaces* **2016**, *8*, 19883−19891.
(15) Criscione, J.; Dobrucki, L.; Zhuang, Z.; Papademetris, X.; Simons, M.; Sinusas, A.; Fahmy, T. Development and Application of a Multimodal Contrast Agent for SPECT/CT Hybrid Imaging. *Bioconjugate Chem.* **2011**, *22*, 1784−1792.
(16) Wu, Y.; Sun, Y.; Zhu, X.; Liu, Q.; Cao, T.; Peng, J.; Yang, Y.; Feng, W.; Li, F. Lanthanide-based Nanocrystals as Dual Modal Probes for SPECT and X-ray CT imaging. *Biomaterials* **2014**, *35*, 4699−4705.
(17) Sun, Y.; Zhu, X.; Peng, J.; Li, F. Core-shell Lanthanide Upconversion Nanoparhosphors as Four-modal Probes for Tumor Angiogenesis Imaging. *ACS Nano* **2013**, *7*, 11290−11300.
(18) Chen, G.; Roy, I.; Yang, C.; Prasad, P. Nanochemistry and Nanomedicine for Nanoparticle-based Diagnostic and Therapy. *Chem. Rev.* **2016**, *116*, 2826−2885.
(19) Smith, B.; Gambhir, S. Nanomaterials for In Vivo Imaging. *Chem. Rev.* **2017**, *117*, 901−986.
(20) Muthu, M.; Leong, D.; Mei, L.; Feng, S. Nanotheranostics-Application and Further Development of Nanomedicine Strategies for Advanced Theranostics. *Theranostics* **2014**, *4*, 660−677.
(21) Luk, B.; Zhang, L. Current Advances in Polymer-based Nanotheranostics for Cancer Treatment and Diagnosis. *ACS Appl. Mater. Interfaces* **2014**, *6*, 21859−21873.
(22) Jo, S.; Ku, S.; Won, Y.; Kim, S.; Kwon, I. Targeted Nanotheranostics for Future Personalized Medicine: Recent Progress in Cancer Therapy. *Theranostics* **2016**, *6*, 1362−1377.
(23) Fan, W.; Yung, B.; Huang, P.; Chen, X. Nanotechnology for Multimodal Synergistic Cancer Therapy. *Chem. Rev.* **2017**, *117*, 13566−13568.
(24) Song, L.; Zhao, N.; Xu, F. Hydroxyl-rich Polycation Brushed Multifunctional Rare-earth-gold Core Shell Nanorods for Versatile Therapy Platforms. *Adv. Funct. Mater.* **2017**, *27*, No. 1701255.
(25) Palivan, C.; Goers, R.; Najer, A.; Zhang, X.; Car, A.; Mejer, W. Bioinspired Polymer Vesicles and Membranes for Biological and Medical Applications. *Chem. Soc. Rev.* **2016**, *45*, 377−411.
(26) Leong, J.; Teo, J.; Aakalu, V.; Yang, Y.; Kong, H. Engineering Polymersomes for Diagnostics and Therapy. *Adv. Healthcare Mater.* **2018**, No. 1701276.
(27) Lee, J. S.; Feijen, J. Polymersomes for Drug Delivery: Design, Formation and Characterization. *J. Controlled Release* **2012**, *161*, 473−483.
(28) Kamaly, N.; Xiao, Z.; Valencia, P.; Radovic-Moreno, A.; Farokhzad, O. Targeted Polymeric Therapeutic Nanoparticles: Design, Development and Clinical Translation. *Chem. Soc. Rev.* **2012**, *41*, 2971−3010.
(29) Wang, F.; Xiao, J.; Chen, S.; Sun, H.; Yang, B.; Jiang, J.; Zhou, X.; Du, J. Polymer Vesicles: Modular Platforms for Cancer Theranostics. *Adv. Mater.* **2018**, *30*, No. 1705674.
(30) Pant, K.; Sedlacek, O.; Nadar, R.; Hruby, M.; Stephan, H. Radiolabelled Polymeric Materials for Imaging and Treatment of Cancer: Quo Vadis? *Adv. Healthcare Mater.* **2017**, No. 1601115.
(31) Elsabahy, M.; Heo, G.; Lim, S.; Sun, G.; Wooley, K. Polymeric Nanostructures for Imaging and Therapy. *Chem. Rev.* **2015**, *115*, 10967−11011.
(32) Zhang, N.; Chen, H.; Fan, Y.; Zhou, L.; Trepout, S.; Guo, J.; Li, M. Fluorescent Polymersomes with Aggregation-induced Emission. *ACS Nano* **2018**, *12*, 4025.
(33) Yang, K.; Liu, Y.; Liu, Y.; Zhang, Q.; Kong, C.; Yi, C.; Zhou, Z.; Wang, Z.; Zhang, G.; Zhang, Y.; Khashab, N.; Chen, X.; Nie, Z. Cooperative Assembly of Magneto-nanovesicles with Tunable Wall Thickness and Permeability for MRI-Guided Drug Delivery. *J. Am. Chem. Soc.* **2018**, *140*, 4666−4677.
(34) Oliveira, H.; Perez-Andres, E.; Thevenot, J.; Sandre, O.; Berra, E.; Lecommandoux, S. Magnetic Field Triggered Drug Release from Polymersomes for Cancer Therapeutics. *J. Controlled Release* **2013**, *169*, 165−170.
(35) Liu, Q.; Song, L.; Chen, S.; Gao, J.; Zhao, P.; Du, J. A Superparamagnetic Polymersome with Extremely High T2 Relaxivity for MRI and Cancer Targeted Drug Delivery. *Biomaterials* **2017**, *114*, 23−33.

DOI: 10.1021/acsami.9b04294
ACS Appl. Mater. Interfaces 2019, 11, 18953−18959

(36) Liu, G.; Liu, X.; Wang, S. Biomimetic Polymersomes as Carriers for Hydrophilic Quantum Dots. *Langmuir* **2012**, *28*, 557−562.
(37) Brinkhuis, R.; Stojanov, K.; Laverman, P.; Eilander, J.; Zuhorn, I.; Rutjes, F.; van Hest, J. Size Dependent Biodistribution and SPECT Imaging of ^{111}In-Labeled Polymersomes. *Bioconjugate Chem.* **2012**, *23*, 958−965.
(38) Wang, G.; Kruijff, R.; Stuart, M.; Mendes, E.; Wolterbeek, T.; Denkova, A. Polymersomes as Radionuclide Carriers Loaded via Active Ion Transport Through the Hydrophobic Bilayer. *Soft Matter* **2013**, *9*, 727−734.
(39) Hu, X.; Zhai, S.; Liu, G.; Xing, D.; Liang, H.; Liu, S. Concurrent Drug Unplugging and Permeabilization of Polyprodrug-gated Cross-linked Vesicles for Cancer Combination Chemotherapy. *Adv. Mater.* **2018**, *30*, No. 1706307.
(40) Zhang, Y.; Wu, K.; Sun, H.; Zhang, J.; Yuan, J.; Zhong, Z. Hyaluronic Acid-shelled Disulfide-cross-linked Nanopolymersomes for Ultrahigh-efficiency Reactive Encapsulation and CD44-targeted Delivery of Mertansine Toxin. *ACS Appl. Mater. Interfaces* **2018**, *10*, 1597−1604.
(41) Jiang, Y.; Zhang, J.; Meng, F.; Zhong, Z. Apolipoprotein E Peptide-directed Chimeric Polymersomes Mediate an Ultrahigh-efficiency Targeted Protein Therapy for Glioblastoma. *ACS Nano* **2018**, *12*, 11070−11079.
(42) Shi, Y.; Jiang, Y.; Cao, J.; Yang, W.; Zhang, J.; Meng, F.; Zhong, Z. Boosting RNAi Therapy for Orthotopic Glioblastoma with Nontoxic Brain-targeting Chimaeric Polymersomes. *J. Controlled Release* **2018**, *292*, 163−171.
(43) You, S.; Jung, H.; Lee, C.; Choe, Y.; Heo, J.; Gang, G.; Byun, S.; Kim, W.; Lee, C.; Kim, D.; Kim, Y.; Kim, Y. High-performance Dendritic Contrast Agents for X-ray Computed Tomography Imaging Using Potent Tetraiodobenzen Derivatives. *J. Controlled Release* **2016**, *226*, 258−267.
(44) Attia, M. F.; Anton, N.; Chiper, M.; Akasov, R.; Anton, H.; Messaddeq, N.; Fournel, S.; Klymchenko, A.; Mely, Y.; Vandamme, T. Biodistribution of X-ray Iodinated Contrast Agent in Nano-emulsion is Controlled by the Chemical Nature of the Oily Core. *ACS Nano* **2014**, *8*, 10537−10550.
(45) Sun, Y.; Hu, H.; Yu, B.; Xu, F. PGMA-based Cationic Nanoparticles with Polyhydric Iodine Units for Advanced Gene Vectors. *Bioconjugate Chem.* **2016**, *27*, 2744−2754.
(46) Yin, Q.; Yap, F.; Yin, L.; Ma, L.; Zhou, Q.; Dobrucki, L.; Fan, T.; Gaba, R.; Cheng, J. Poly(iohexol) Nanoparticles as Contrasts Agents for In Vivo X-ray Computed Tomography Imaging. *J. Am. Chem. Soc.* **2013**, *135*, 13620−13623.
(47) Lee, J.; Chung, S.; Cho, H.; Kim, D. Iodinated Hyaluronic Acid Oligomer-based Nanoassemblies for Tumor-targeted Drug Delivery and Cancer Imaging. *Biomaterials* **2016**, *85*, 218−231.
(48) Zou, Y.; Wei, Y.; Wang, G.; Meng, F.; Gao, M.; Storm, G.; Zhong, Z. Iodine-Rich Nano-Polymersomes as a High-Performance X-Ray Computed Tomography Contrast Agent. *Adv. Mater.* **2017**, *29*, No. 1603997.
(49) Zhao, L.; Zhu, J.; Cheng, Y.; Xiong, Z.; Tang, Y.; Guo, L.; Shi, X.; Zhao, J. Chlorotoxin-conjugated Multifunctional Dendrimers Labeled with Radionuclide ^{131}I for Single Photon Emission Computed Tomography Imaging and Radiotherapy of Gliomas. *ACS Appl. Mater. Interfaces* **2015**, *7*, 19798−19808.
(50) Cheng, Y.; Zhu, J.; Zhao, L.; Xiong, Z.; Tang, Y.; Liu, C.; Guo, L.; Qiao, W.; Shi, X.; Zhao, J. ^{131}I-labeled Multifunctional Dendrimers Modified with Bmk CT for Targeted SPECT Imaging and Radiotherapy of Giomas. *Nanomedicine* **2016**, *11*, 1253−1266.
(51) Zhu, J.; Zhao, L.; Cheng, Y.; Xiong, Z.; Tang, Y.; Shen, M.; Zhao, J.; Shi, X. Radionuclide ^{131}I-labeled Multifunctional Dendrimers for Targeted SPECT Imaging and Radiotherapy of Tumors. *Nanoscale* **2015**, *7*, 18169.
(52) Mei, K.; Bai, J.; Lorrio, S.; Wang, J.; AI-Jamal, K. Investigating the Effect of Tumor Vascularization on Magnetic Targeting In Vivo Using Retrospective Design of Experiment. *Biomaterials* **2016**, *106*, 276−285.
(53) Perry, J.; Reuter, K.; Luft, J.; Pecot, C.; Zamboni, W.; DeSimone, J. Mediating Passive Tumor Accumulation Through Particle Size, Tumor Type, and Location. *Nano Lett.* **2017**, *17*, 2879−2886.
(54) Ojha, T.; Pathak, V.; Shi, Y.; Hennink, W.; Moonen, C.; Strom, G.; Keissling, F.; Lammers, T. Pharmacological and Physical Vessel Modulation Strategies to Improve EPR-mediated Drug Targeting to Tumors. *Adv. Drug Delivery Rev.* **2017**, *119*, 44−60.
(55) Zhang, Z.; Kuijer, R.; Bulstra, S. K.; Grijpma, D.; Feijen, J. The In Vivo and In Vitro Degradation Behavior of Poly(trimethylene carbonate). *Biomaterials* **2006**, *27*, 1741−1748.
(56) Yang, L.; Li, J.; Meng, S.; Jin, Y.; Zhang, J.; Li, M.; Guo, J.; Gu, Z. The In Vivo and In Vitro Degradation Behavior of Poly-(trimethylene carbonate-co-ε-caprolactone) implants. *Polymer* **2014**, *55*, 5111−5124.

DOI: 10.1021/acsami.9b04294
ACS Appl. Mater. Interfaces 2019, 11, 18953−18959